Valorization of not soluble byproducts deriving from green keratin extraction from poultry feathers as filler for biocomposites

E. Pulidori[1], S. Micalizzi[2], E. Bramanti[3], L. Bernazzani[1], C. De Maria[2*], C. Pelosi[1*], M. R. Tinè[1], G. Vozzi[2] and C. Duce[1]

[1]: Department of Chemistry and Industrial Chemistry, University of Pisa, Via G. Moruzzi 13, 56124 Pisa, Italy

[2]: Research Centre E. Piaggio and Department of Information Engineering, University of Pisa, Largo L. Lazzarino 1, 56126 Pisa, Italy

[3]: Institute of Chemistry of Organometallic Compounds, National Research Council, via G. Moruzzi 1, 56124 Pisa, Italy

*: Corresponding authors. E-mail: carmelo.demaria@unipi.it, chiara.pelosi@dcci.unipi.it

ABSTRACT

The valorization of poultry feathers wastes is very important to reduce the environmental pollution deriving from their disposal. In this frame, we present the production process of completely natural, biodegradable, biocompatible and eco-friendly composites made by non-soluble keratin (NSK) and poly(lactic acid) (PLA).
NSK was obtained as by-product of a microwave assisted keratin extraction from poultry feathers and it was added to PLA pellets without adding additional compatibilizers or plasticizers, differently from the other works reported in the literature until now. The mixture was used to obtain homogeneous NSK-based PLA filaments by means of hot-melt extrusion technology. The filaments were subsequently 3D printed to explore applications in the additive manufacturing field. All the samples presented unaltered thermal stability, but reduced toughness with respect to neat PLA. Other tested parameters (water adsorption, glass transition, crystallinity) were dependent from NSK content and from the fabrication technology. Besides, Fourier Transform Infrared Spectroscopy (FTIR) highlights the differences in the structure of the NSK-based PLA filaments and 3D printed samples.

KEYWORDS: PLA biocomposites, keratin, microwave-assisted extraction, poultry feathers valorization, circular economy.

1. INTRODUCTION

The modification of polymeric materials properties by adding fibers of various sources and in different concentrations is a strategy highly explored in the last decades. There are two types of fibers mainly used as polymeric materials fillers: synthetic fibers (e.g. glass [1], aramid [2], carbon [3], quartz [4], boron [5] or ceramic [6]) and natural fibers (obtained from animals [7], minerals [8], or plants [9]). Even though synthetic fibers possess higher mechanical properties, natural fibers are abundant, economic, biodegradable, renewables and eco-friendly, therefore they are preferred to prepare new generation composite materials. Fibers obtained from plants (e.g., bamboo, cotton, jute or pineapple) and animals (e.g. feathers) have been extensively studied as fillers of different plastics [10]. In this frame, the use of fibers obtained from waste materials is highly desirable with the aim to develop new processes following circular economy principles. Poultry feathers (which contain more than 90% of keratin) have raised some interest for their high availability, and for the high amount of keratin contained. The valorization of keratin from feathers has a high economic impact because it is proposed as alternative to the common disposal strategies (usually landfill and incineration), expensive and not eco-friendly [11].
Keratin is a structural protein characterized by a high sulfur and hydroxyl amino acid content, due to the high amount of cysteine and serine residues, respectively. In the native form, it is usually tightly packed in quaternary structures called coiled coils, and it shows high tensile mechanical stability and high resistance to the attack of external agents. These features, together with its biocompatibility, make it appealing for various biomedical or technological applications [12]. Keratin fibers have already been used as filler of several polymers, using either ground feathers or extracted keratin in solution [13]. For this purpose, various keratin extraction methods from waste materials have been already reported in the literature, including sulpholysis [14,15], alkaline [16] or enzymatic [17] extractions, which, anyway, are highly disruptive. We have recently reported an innovative and green keratin extraction from waste feathers, in which the raw hydrolyzed soluble keratin was blended with gelatin and used to prepare bioplastics by electrospinning procedure [18]. As a byproduct of the process, we obtained a high quantity of not-soluble keratin (NSK).
Following the circular economy principles and in view of a complete utilization of all the materials recovered, we propose, in the present work, the valorization of the not-soluble keratin (NSK) obtained from our microwave assisted acidic extraction [18] as fillers of polylactic acid (PLA), processed by hot melt extrusion (HME). The filaments obtained were subsequently 3D printed by fused deposition modelling (FDM) 3D printing technology.

Figure 1. Scheme of the valorization of keratin from waste poultry feathers obtaining soluble keratin and keratin/PLA composites.

Due to its thermomechanical properties, biodegradability, and biocompatibility, PLA is a sustainable alternative to petrochemical products [19], already used for several applications, including food packaging [20], water and milk bottles [21], degradable plastic bags [22], drug delivery [23], tissue engineering [24], aerospace [25], and automotive [26]. PLA is considered a benchmark for the loading of keratin fibers on bioplastic materials. Hydrolysed keratin or ground feathers from various sources have been added to PLA, and the properties of the materials have been studied [13]. For instance, Puglia and co-workers used three different keratin sources (Merino wool, Brown Alpaca fibres and commercial hydrolysed keratins) as fillers in PLA based biocomposites via solvent casting in chloroform, showing the dependence of the material properties on the keratin source [27]. In a similar manner, the influence of chicken feathers on PLA matrix depends on feather pre-treatment, keratin quantity and manufacturing technology used. Huda et al. prepared PLA/poultry feather keratin (70/30) composite materials by melt extrusion, finding improved mechanical properties (flexural and tensile moduli) with respect to neat PLA [28]. Similarly, Spiridon and co-workers observed that the addition of feather keratin fibers (2–4 wt. %) to PLA/chitosan matrix, improved thermal stability, elastic modulus, tensile and impact strength of the samples prepared by compression molding, but it decelerates its degradation [29]. On the other hand, PLA + chicken feathers consolidated in a hot plate press machine showed a decrease of the tensile strength and elongation with increasing the quantity of added feathers [30]. Aranberri et al. produced materials based on PLA copolymer blends, with much higher loadings of chicken feather fibers (50 and 60 wt. %), manufactured with a torque rheometer. In this case, the thermal stability, tensile strength and elongation-at-break of the materials were negatively affected by the feathers presence [31]. It is worth noticing that in all these cases, the addition of feather fibers to PLA requires the use of a compatibilizer (e.g. polyethylene glycol [31], 3-aminopropyltriethoxysilane or polybutadiene [28]) or a feather pre-treatment using acid [32] or alkali [28,33] conditions, to improve the interphase adhesion among keratin fibers and PLA.
In this work, NSK extracted in 2 hours with a microwave coaxial antenna was extensively characterized using differential scanning calorimetry, thermogravimetry, scanning electron microscopy, and Fourier transformed infrared spectroscopy, highlighting the differences with the raw feathers. NSK was then mixed with PLA at different concentrations and extruded by hot-melt extrusion technology. NSK-filled PLA filaments were finally used for 3D printing, highlighting the applications in the additive manufacturing field.

2. MATERIALS AND METHODS

Poultry feathers were provided by Consortium SGS (Santa Croce sull' Arno, Italy), as poultry treatment byproduct. Acetic acid (ACS grade) was purchased from Sigma-Aldrich (Milan, Italy). Black PLA filament with a diameter ø = 1.75 mm was purchased from Filoprint (Florence, Italy).

2.1 Keratin extraction

Not-soluble keratin (NSK) was obtained by a procedure described in a previous works [18]. In brief, 12 g of ground feathers were put in 800 mL of acetic acid (70% v/v), in a microwave (MW)-assisted extractor device. A MW coaxial dipole antenna supplied continuous MW irradiation power until reflux temperature (104 °C), which was maintained for 2 hours. Later, the reaction broth was allowed to cool at room temperature, and it was sieved with steel sieve (cut off 500 µm) to separate unconverted feathers. The suspension was centrifuged at 8000 rpm for 10 minutes. The supernatant was eliminated, and the solid residue (NSK) was washed in water until to neutralization (pH =7) and centrifuged again in the same conditions for three times. Finally, the residue was collected and dried in the oven at 60 °C. Further details are reported in ref. [18].

2.2 Scanning Electron Microscope Analysis (SEM)

The microscopic structure of NSK was analyzed by FEI Quanta 450 ESEM FEG (Bruker), prior metalizzation with platinum using Leica EM ACE600 metallizer.

2.3 Composite preparation and filament fabrication

Pellets of PLA and NSK powder were weighted, transferred into a beaker, and manually mixed until homogenization. Filaments of neat PLA and NSK-filled PLA at NSK different concentrations (1%, 2% and 4%(w/w)) were fabricated by hot-melt extrusion (HME) technology [34] using a Felfil Evo extruder (Felfil, Turin, Italy). The extruder is composed by a single rotating screw located inside a stationary heated cylindrical barrel. An endplate with a 1.75 mm diameter die

connected at the end of the barrel. An extrusion temperature of 187 °C and, a screw rotating speed 6 RPM were selected. An air-cooling system and a manual spooling were used.

2.4 Physical characterization

After the extrusion process, the filament diameter was measured in at least n = 6 points for each filament. Studies on the density and the water absorption of the fabricated filaments were performed.

The density ρ [gr·cm^{-3}] was evaluated collecting n = 3 samples of length L = 50 mm from each extruded filament and weighting them using an analytical balance (Mettler Toledo AE240).

The water absorption was determined by immersion of the specimens vertically in distilled water at two different temperatures T_1 = 25 °C and T_2 = 50 °C for 2 h. Specimens were cut with a length L = 50 mm. Once extracted from water, samples were wiped with paper to remove the excess of water on the surface and weighted. Measurements were made in triplicate. The percentage of water absorption (WA in %) was calculated using following equation (Eq. 1):

$$\mathrm{WA}(\%) = \frac{\text{wet mass} - \text{dry mass}}{\text{dry mass}} \cdot 100 \qquad \text{(Eq. 1)}$$

2.5 Sample Design, slicing and printing parameters

3D printed samples were fabricated starting from NSK-filled PLA at different concentration (1%, 2%, 4% w/w%) using the FDM 3D printing process. Pure PLA filament was used as control. In particular, the shape of the samples was specifically designed for the mechanical 3-point bending testing according to the ISO 178: 2019, which suggests a working length L_0 equal to $16 \cdot h$, where h is the specimen thickness.

Slic3r® software was used to analyse the .STL files and produce the file for the 3D printing process, performed using a 3D printer Geeetech A10M from Geeetech® (Shenzhen, China). Slicing and printer parameters are listed in Table 1 and were set to ensure that all the strands of the 3D printed sample were aligned to the stress induced by the bending load.

Table 1. Design, slicing and printing parameters.

Parameters	Settings	Unit
Specimen size (L x w x h)	52 x 4.5 x 3	mm
Infill	100	%
Layer thickness (Total layers n = 15)	0.2	mm
Printing speed	40	mm/s
Infill pattern	Rectilinear	/
Infill direction	90	degrees with X axis
Nozzle diameter	0.4	mm
Nozzle temperature	205	°C
Bed temperature	60	°C

2.6 Mechanical characterization

The mechanical characterization was carried out performing a three-point flexural test both on extruded filaments and 3D printed beams.

Tests were performed using a universal machine Zwick-Roell Z005 ProLine equipped with a 100N load cell. Samples were tested in triplicate until failure, setting a strain rate calculated according to the ISO 178: 2019, using Eq. 2:

$$\dot{\varepsilon} = \frac{\varepsilon' \cdot L_0^2}{6h} \qquad \text{(Eq. 2)}$$

where, ε' = 1 %/min is the deflection rate suggested for samples with a thickness h < 3 mm (for the filament samples, the diameter ø (mm) was considered), L_0^2 (m) is the squared working length. Load F [N] and deflection Δx [m] of the centre of the specimen were recorded from the machine and, from these data, the flexural modulus E_f [MPa], the failure stress σ_f [MPa], the corresponding failure strain ε_f [%], and toughness U [J·m^{-3}] were calculated. For the mechanical characterization of the extruded filaments following equations were used:

$$E_f = \frac{4\alpha \cdot L_0^3}{3\pi\phi^4} \quad \text{(Eq.3)}$$

$$\sigma_f = \frac{16FL_0\phi}{\pi\phi^4} \quad \text{(Eq. 4)}$$

$$\varepsilon_f = \frac{6\phi\Delta x}{L_0^2} \quad \text{(Eq. 5)}$$

where, α is the slope of the first linear portion of the load deflection curve (N/mm). For the characterization of the 3D printed beams the following equations were used:

$$E_f = \frac{\alpha \cdot L_0^3}{4wh^3} \quad \text{(Eq. 6)}$$

$$\sigma_f = \frac{3FL_0}{2wh^2} \quad \text{(Eq. 7)}$$

$$\varepsilon_f = \frac{6h\Delta x}{L_0^2} \quad \text{(Eq. 8)}$$

Where, w [m] and h [m] are respectively the samples width and the thickness, as indicated in Table 1.

2.7 Thermogravimetry (TG)

Thermogravimetry measurements were performed on raw feathers, NSK, PLA, and extruded and printed NSK-filled PLA biocomposites at a rate of 10 °C min^{-1}, from 25 to 600°C or to 900 °C under nitrogen flow (25 mL min^{-1}) with a TA Instruments Thermobalance model Q5000IR, using 2-5 mg of sample. The measurements were repeated at least 3 times for exemplificative samples, sampling the materials in different points, to assess their homogeneity.

2.8 Differential scanning calorimetry (DSC)

DSC experiments were carried out on raw feathers, NSK, PLA, and extruded and printed NSK-filled PLA biocomposites by TA Instruments Discovery DSC model 250 under the nitrogen gas flow 50 mL·min^{-1}. Each sample (3-5 mg) was weighted and hermetically sealed into an aluminum DSC pan. A heating-cooling cycle from 25 to 200 °C at 10 °C/min, followed by a second heating scan in the same conditions was performed. The instrument was calibrated with Indium, and an empty pan was used as a reference. All the thermal parameters were obtained from the second heating curves to eliminate the contribution of the sample thermal history.

The degree of crystallinity was calculated in relation to the effective PLA weight in the bio composites, using the following equation, as described in the cited reference [31]:

$$X_c(\%) = \frac{100}{\Delta H_{m,s}^0} \cdot \frac{\Delta H_m - |\Delta H_c|}{w} \quad \text{(Eq. 9)}$$

where $\Delta H_m - |\Delta H_c|$ is the difference between the observed melting enthalpy and the absolute value of cold crystallization enthalpy and $\Delta H_{m,s}$ is the estimated specific melting enthalpy of the pure PLA (93.7 J/g) [35]. The measurements were repeated at least 3 times for exemplificative samples, sampling the materials in different points, to assess their homogeneity.

2.9 Fourier Transform Infrared Spectroscopy

Infrared spectra were recorded by using a Perkin-Elmer Frontiers FTIR Spectrophotometer, equipped with a universal attenuated total reflectance (ATR) accessory and a triglycine sulphate TGS detector. Measurements on NSK, PLA and extruded and printed NSK-filled PLA biocomposites (N=3 replicates) were performed in ATR mode after background acquisition. For each sample, 128 scans were recorded, averaged and Fourier-transformed to produce a spectrum with a nominal resolution of 4 cm^{-1}. A written-in-house LabVIEW program for peak deconvolution were employed to process the spectra. The LabVIEW program for peak fitting is described elsewhere [36]. Secondary structures were estimated by

expressing the amplitude value of the bands assigned to each of these structures as a fraction of the total sum of the amplitudes of the amide I components [37–39].

2.10 Data processing and statistical analysis

Data are presented as mean ± standard deviation. For the thermal, physical and mechanical characterization, statistical comparisons were performed using two-tailed t-student test with a p-value < 0.05.
Principal component analysis (PCA) was carried out on the chemical data, after column autoscaling, to investigate possible clustering of samples. The ATR spectra were standardized by using standard normal variate (SNV) in order to minimize unwanted contributions (e.g. global intensity effects or baseline shifts), then silent regions were removed. The analysis was carried out through the software XLStat 2021.2.1 (Addinsoft 2021. XLSTAT statistical and data analysis solution. New York, USA).

3. RESULTS

3.1 NSK characterizations

The morphology study of the NSK highlighted a more degraded structure than the feather even though the typical structure of rachis and barbs is observable even at micrometric level (Fig. 2a). At 500x magnification (Fig. 2a) the medullary matrix is visible, present as a component within the rachis, while at 16000 x magnification (Fig.2b) it is possible to observe filaments, dispersed in the amorphous matrix.

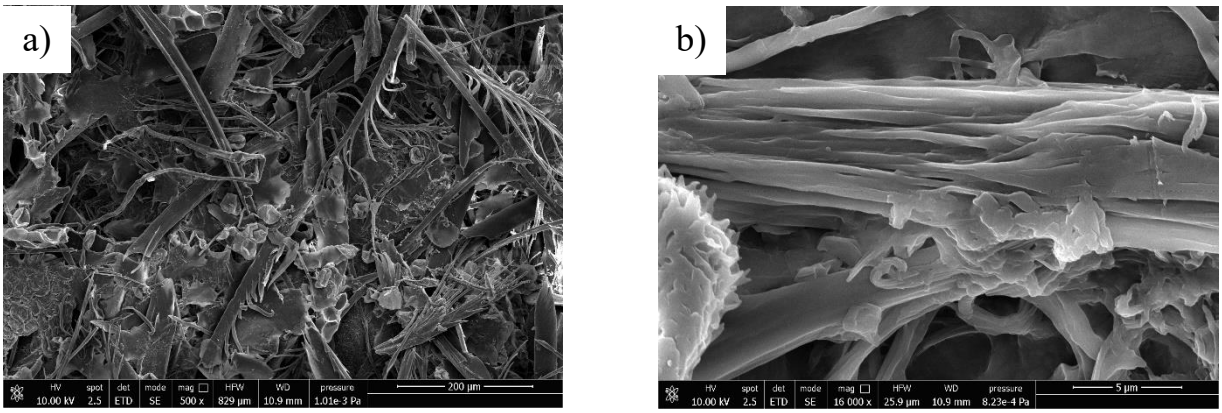

Figure 2. SEM images of NSK: **a**-500x magnification, **b**-16000x magnification.

The TG analysis of NSK shows comparable degradation pattern for poultry feathers and NSK. There are two distinct steps of mass loss. The first one occurs below 100°C and corresponds to evaporation of adsorbed water (6-7 wt%) while the second that occurs between 180 °C and 550 °C (69 wt% NSK *vs* 75 wt% feathers) is due to keratin degradation. A shoulder is observed between 220 and 240 °C, both for NSK and feathers, and it is attributable to disulphide bridge cleavage of crosslinked cystines which are a distinctive feature of keratin compared to other proteins. The melting of crystalline part and the formation of aromatic carbons and cyclic amines occurs above 250 °C while the degradation of cyclic and aromatic framework occurs above 400 °C and up to 600 °C [40]. The residue at 600 °C is about 24% for NSK and 17% for feathers. The results obtained for the feathers agree with literature data [40].
Observing the DTG curves, the NSK exhibit a thermal stability slightly higher than poultry feathers as the temperature of the second mass loss is slightly greater, as clearly visible comparing the curves' maximum (330 °C vs. 318 °C).
The DSC curves show an unfolding peak at 70.4 °C ($\Delta H = 2.25$ J/g) and 58.8 °C ($\Delta H = 2.91$ J/g) for poultry feathers and NSK, respectively. We can hypothesize that the low unfolding temperature observed in the NSK is related to a more degraded structure with respect to feathers, which determines the early onset of the process.

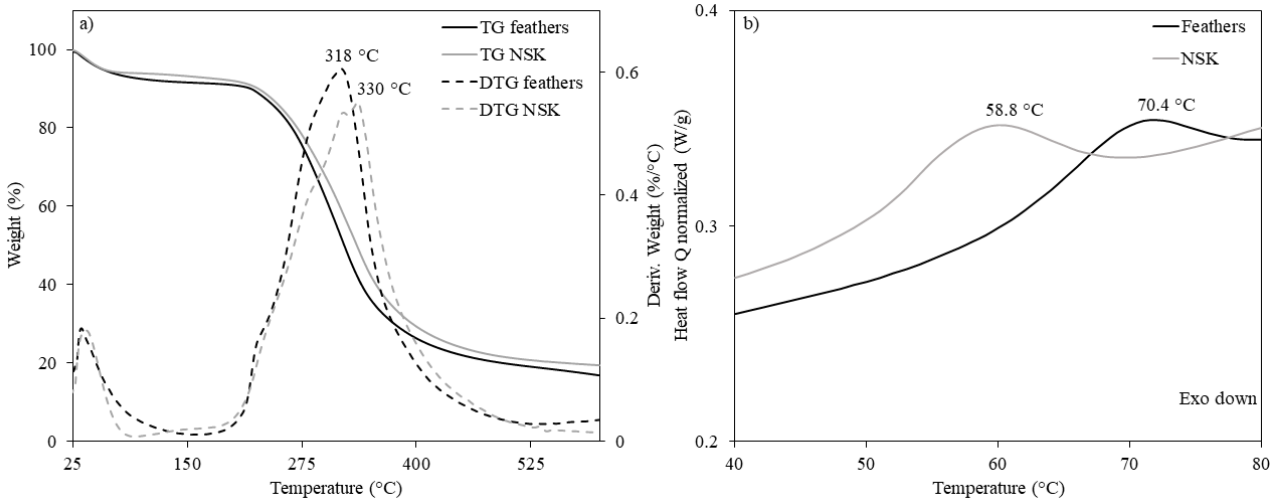

Figure 3. Thermogravimetric curves (a) and calorimetric curves (b) of poultry feathers and NSK under nitrogen flow

Figure 4 shows representative ATR-FTIR spectra of NKS and raw feathers. The spectra have different and reproducible features.

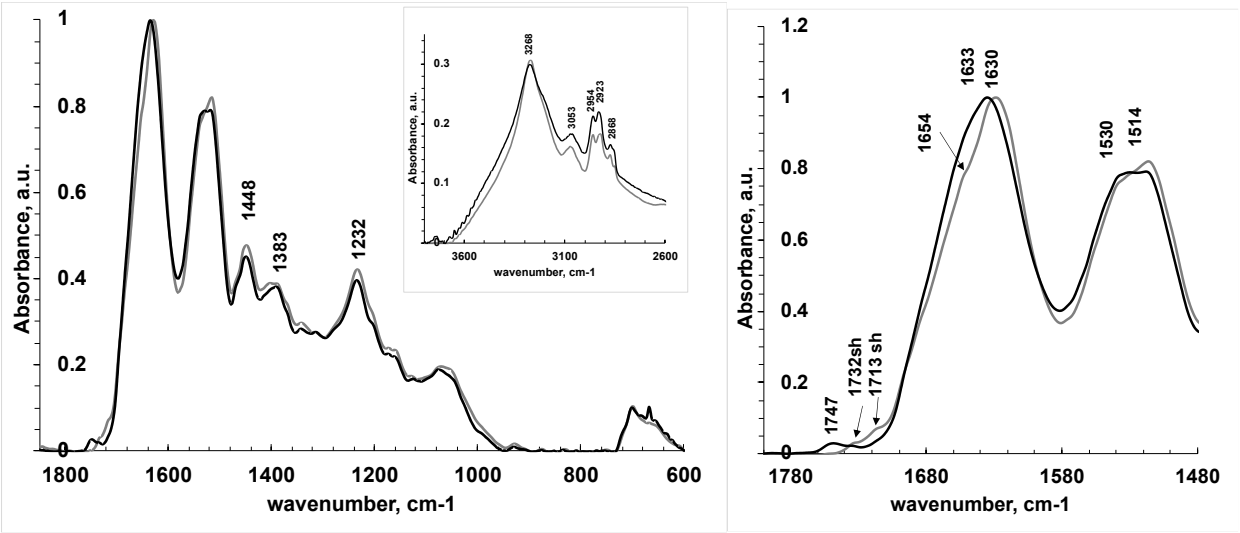

Figure 4. ATR-FTIR absorption spectra in the 1850-600, 4000-2600 and 1800-1480 cm^{-1} regions of NKS (gray line) and feather (black line).

The broad band located between 3650–3050 cm^{-1} is assigned to the O-H and N-H stretching vibration of keratin. We also observe the stretching vibrations of CH_2 and CH_3 groups present in keratin amino acid side chains and of residual fat in feather spectrum, evidenced in the latter also by the band at 1747 cm^{-1} due to the stretching of carbonyl group of the aliphatic ester. In this region of the spectrum the NSK have two shoulders at 1732 and 1713 cm^{-1}. The first one is due the C=O stretching of the ester bond, which suggests the acetylation of several keratin groups, due to its extraction in 70% acetic acid [41]. The band at 1713 cm^{-1} might be associated with residual traces of acetic acid. Acetylation is confirmed also by the appearances of a new component in the Amide II band at 1514 cm^{-1} and by the appearance of the shoulder at 1654 cm^{-1} [41].

The characteristic main absorptions of the amide groups of proteins are observed at 1633 -1630 cm^{-1} (amide I, due to amide C=O stretching) and at 1530-1514 cm^{-1} (amide II due to the N–H bending). The amide I region is generally used to investigate quantitative changes in protein secondary structure by a peak deconvolution or recognition pattern approaches and the peak at 1633 cm^{-1} is associated with beta structure [36,42].

By applying the deconvolution procedure to the amide I region of the FTIR spectra, the percentage of each amide I component was obtained. Figure 5 summarizes the quantitative results of the secondary structure of NSK and raw feathers. Each single component has been assigned to a specific secondary structure based on the literature data [36,42].
The main result is the significant decrease of the component assigned to α-helix at 1658 cm^{-1} from 34.9 ± 3 to 23.7± 1. This decrease could be even bigger considering the not quantifiable contribution of acetylation band to the component at 1658 cm^{-1} .

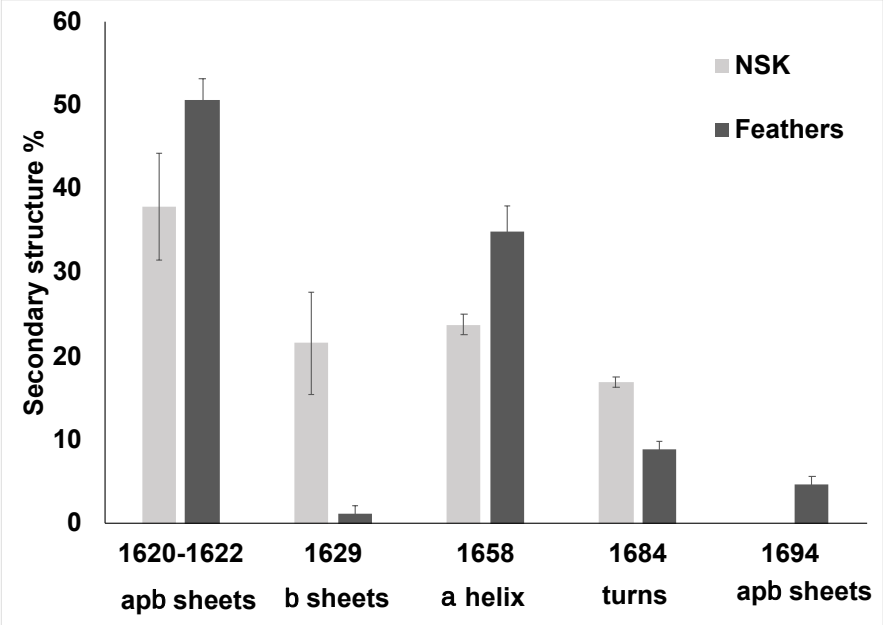

Figure 5. Secondary structure percentages resulting from the deconvolution procedure applied to the amide I region of the FTIR spectra of NSK and raw feathers (N=3 replicates).

3.2 PLA/NSK bio composites characterizations

3.2.1 Keratin/PLA compatibility

The lack of compatibility of keratin obtained from poultry feathers with the desired polymer matrix is one of the most critical issues in the processability of a new material [13]. Different studies have reported the necessity of keratin pre-treatments to guarantee a good compatibility with PLA, e.g. using acid [32] or alkali [28,33] treatment of the feathers, or adding other polymers (as polyethylene glycol [31], 3-aminopropyltriethoxysilane or polybutadiene [28]) as compatibilizer.
In this work, the extraction procedure applied to the poultry feathers [18] allows obtaining NSK which can be used straightforwardly as a PLA filler, as it shows high compatibility with the polymer and a good dispersion also during the manual mixing before the HME process, without the use of any compatibilizer. A possible explanation can be carried out considering an electrostatic interaction between PLA and acetylated Keratin constituting NSK. PLA presents negative surface potential (-21 mV) [43]. Keratin from wool in water is reported to have a zeta potential of -3mV [44].The acetylation of keratin, assessed by ATR in our case, could shift this value toward a positive one. This high compatibility was also confirmed by the homogeneity of the final filament and the 3D printed specimens, as shown by the low error obtained for the DSC and TGA replica performed, sampling in different points of the materials.

3.2.2 Physical characterization

Fabricated filaments appear rougher on the surface as the NSK content increases with respect to the pure PLA filament. We evaluated the density of the filaments (around 1g/cm^3), which do not significantly differ in PLA and NSK- PLA filaments.
We observed an increasing water absorption (WA) for increasing percentages of NSK in the composites. After 2h of immersion in water the WA was about 6% bigger for samples with a 4% w/w NSK concentration with respect to pure PLA. These results agree with the ones published by Aranberri et al. [31] where, researchers measured a 16% of increasing

of WA in composites with keratin concentration around 50% (w/w). We also investigated the effect of the increasing in temperature that seams do not affect the samples water absorption.

3.2.3 Mechanical characterization of extruded and 3D printed samples

Figure 6 shows the fabrication process of NSK-PLA 3D structures.

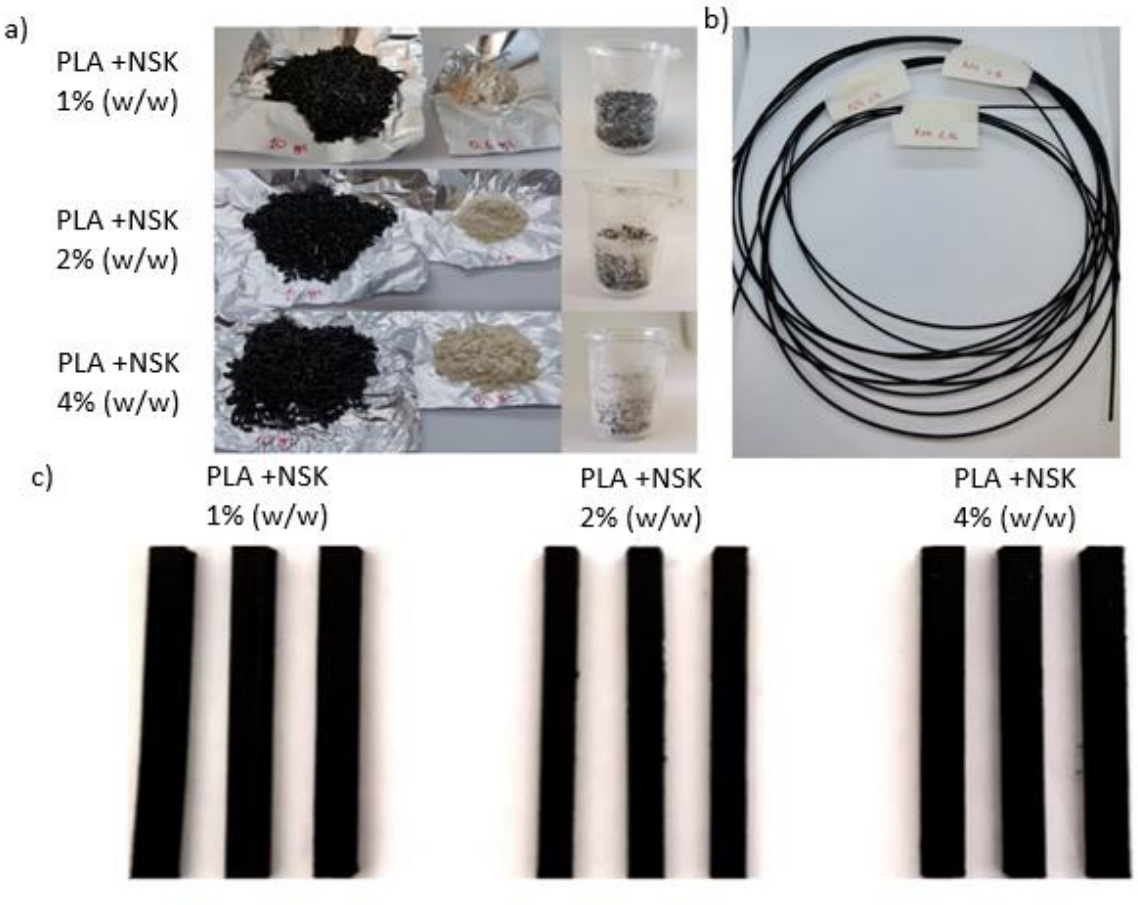

Figure 6. Illustration of the PLA-NSK structures fabrication process: (a) compounds preparation and mixing, (b) extruded filaments, and (c) 3D printed specimens.

Extruded filaments and 3D printed beams (Fig. 6(c)) were mechanically tested running a 3-point bending test. Results are listed in Table 2.

Table 2. Values of maximum flexural stress σ_f (MPa), maximum flexural strain ε_f (%), flexural modulus E_f (GPa), and toughness U ($J \cdot m^{-3}$) for all the fabricated and tested filaments and beams.[(a)]

	Maximum flexural stress σ_f		**Maximum flexural strain ε_f**		**Flexural Modulus E_f**		**Toughness U**	
	Filament (MPa)	**Beam** (MPa)	**Filament** (%)	**Beam** (%)	**Filament** (MPa)	**Beam** (GPa)	**Filament** 10^5 ($J \cdot m^{-3}$)	**Beam** 10^6 ($J \cdot m^{-3}$)
PLA	90 ± 10	90 ± 5	4 ± 0.5	4 ± 0.1	48 ± 18	3.1 ± 0.6	3 ± 0.1	4 ± 0.4
PLA/NSK 1%(w/w)	66 ± 8	66 ± 13	6 ± 0.3	3 ± 0.5	43 ± 14	2.7 ± 0.4	3 ± 0.6	2 ± 0.6
PLA/NSK 2%(w/w)	26 ± 12	63 ± 9	4 ± 1	3.5 ± 0.2	24 ± 12	2.6 ± 0.1	1 ± 0.3	2 ± 0.3
PLA/NSK 4%(w/w)	12 ± 4	63 ± 9	3 ± 1	3.2 ± 0.2	17 ± 6	3 ± 0.2	0.3 ± 0.1	1.6 ± 0.9

[(a)]Data are reported as mean ± standard deviation.

Analyzing results from flexural tests for both extruded filaments and 3D printed beams, a decreasing of the mechanical performance of the NSK-filled PLA samples compared to pure PLA is highlighted. For the extruded filaments, a decreasing of the evaluated parameters is also registered increasing NSK concentration. Differently, 3D printed beams do not show this dependence. This can be explained considering the 3D printing process. During printing process, in fact, filaments are forced to pass from a nozzle with a significantly smaller diameter (0.4 mm). This may better reorganize the filler inside the PLA matrix. The printing parameters also play an important role. In fact, the possibility to print multiple layers (n = 15) with the same thickness (0.2 mm) and characteristics improves the mechanical performance of the 3D structure. Both printing technology and printing parameters flatten the difference among sample with different NSK concentration. This behavior is shown in Figure 7 taking as example the maximum flexural stress and the toughness comparing obtained values for both structures.

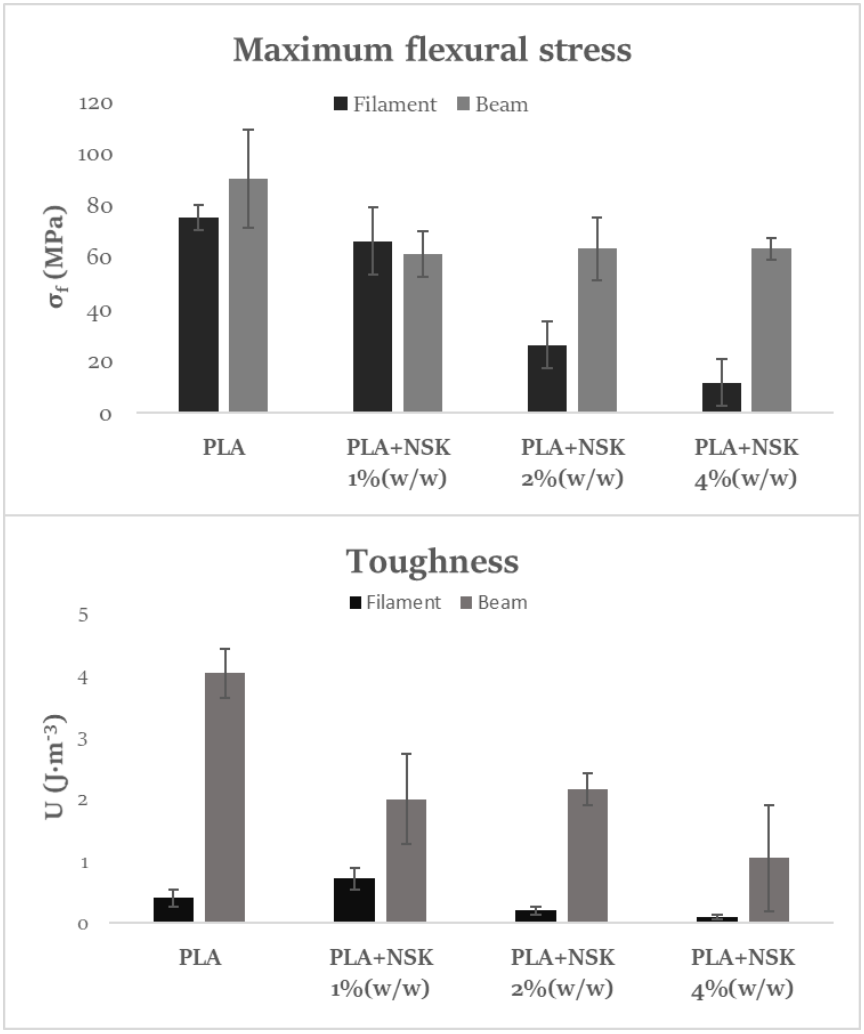

Figure 7. Maximum flexural stress (up) and toughness (down) parameters comparison: extruded filaments (black) and 3D printed beams (gray).

NSK-filled PLA beams presented a decreasing of about 30% in flexural stress and toughness (Fig. 7) comparing with pure PLA materials. This behavior was already investigated by Huda et al [28] that measured the same decreasing percentage for these parameters.

3.2.3 FTIR Analysis

Figure 8 shows representative ATR-FTIR spectra of extruded (E) and printed (P) PLA and NSK-filled PLA composite.

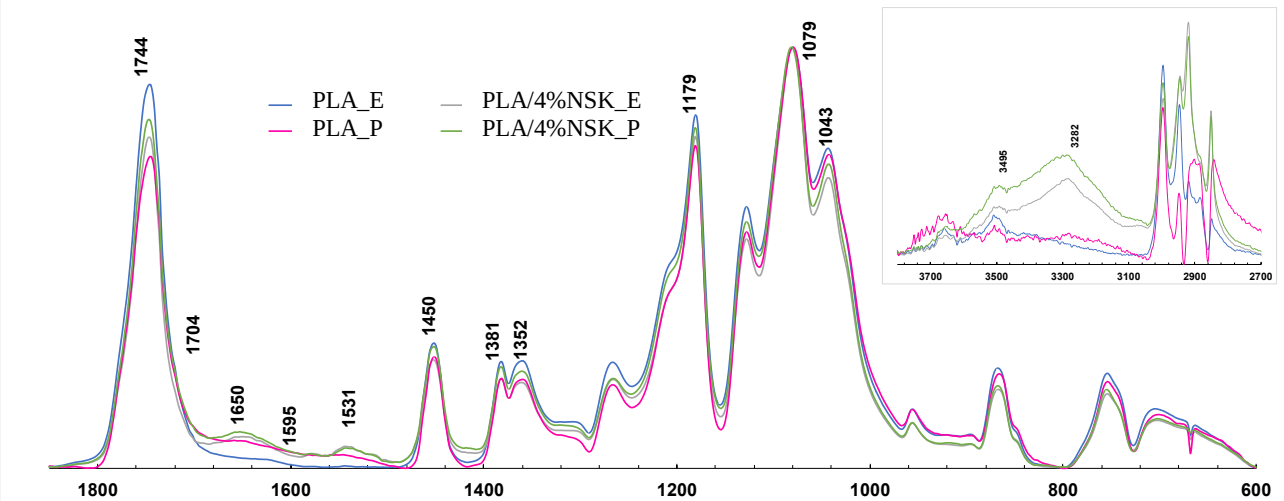

Figure 8. Representative ATR-FTIR spectra of extruded (E)and printed (P) PLA and PLA/keratin composite in 3800-2700 and 1850-600 cm^{-1} region.

The typical peaks of the keratin in the O-H (3292 cm^{-1}) and N-H stretching region (3503 cm^{-1}), and in the amide I at 1650 cm^{-1} and amide II region at 1531 cm^{-1} were detected in NSK-PLA biocomposite samples and the intensity of the peaks increased with keratin loading as a proof of keratin presence and its incorporation into the polymer matrix.
Figure 9 reports the results of PCA performed in the 1850-800 cm^{-1} that show a separation between printed and extruded samples.

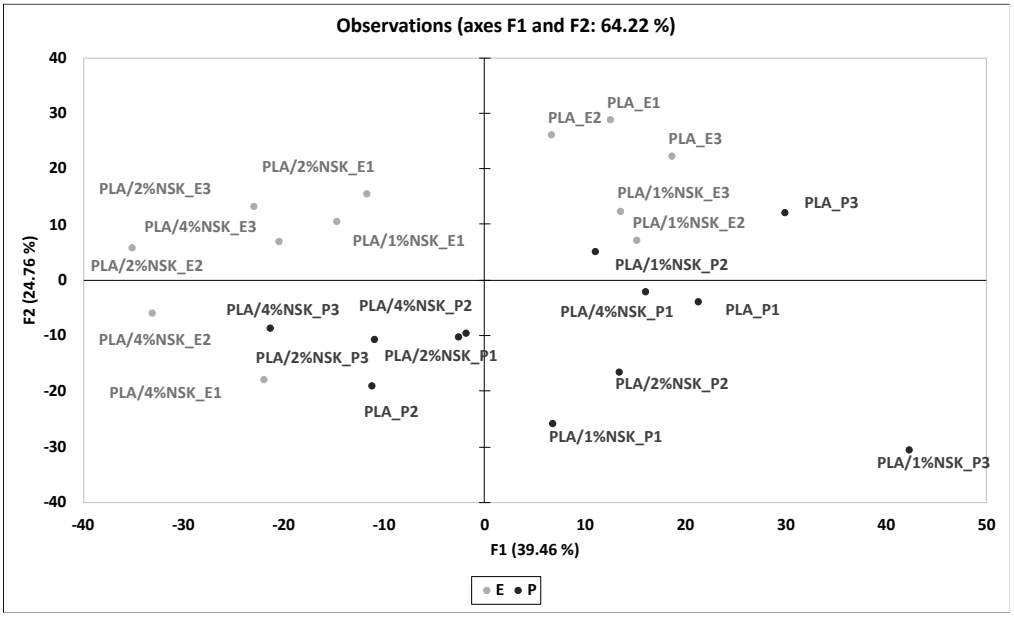

(A)

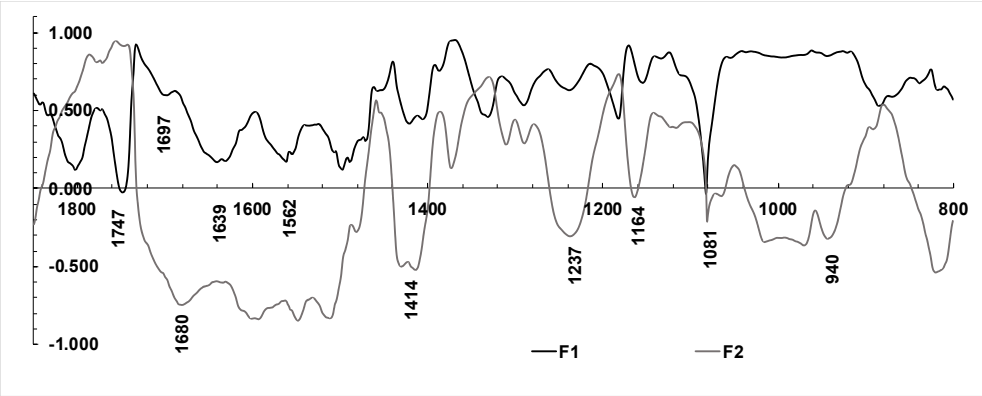

(B)

Figure 9. PCA performed on extruded and printed PLA and NSK-PLA biocomposite FTIR spectra (1850-800 cm-1 region). The score (A panel) and the loading plot (B panel) were reported. N=3 replicates are reported for each type of samples (E and P PLA and E and P PLA with 1, 2 and 4 % NSK).

The loading plot (Figure 9B) shows that the separation between this set of samples is due both to keratin absorptions in the amide regions (1700-1480 cm^{-1} region and 1237 cm^{-1} band, amide III) and in the PLA bands (1850-1700 and 1300-600 cm^{-1} region).

This separation is basically due to two phenomena: (i) the variation in crystallinity of PLA; (ii) the changes in the NS keratin secondary structure. In the C=O stretching region, it is reported that perfectly flat crystals of PLA give two narrow components at 1767 and 1758 cm^{-1}, and skeletal band at 955 cm^{-1} [45]. Here the loading plot evidenced peaks at 1747 cm^{-1}, at 940 cm^{-1} and changes in the 1200-800 cm^{-1} region.

To investigate possible changes in the secondary structure of keratin in NSK-PLA biocomposite the peak fitting was applied to the amide I band of 4% NSK-filled PLA sample. Figure 10 shows the secondary structure percentages resulting from the deconvolution procedure applied to the amide I region of the FTIR spectra of 4% NSK-filled extruded (E) and printed (P) PLA composites. The biocomposites with 4% NSK were considered for this analysis as the intensity of the amide I band is good enough to guarantee a reliable data processing.

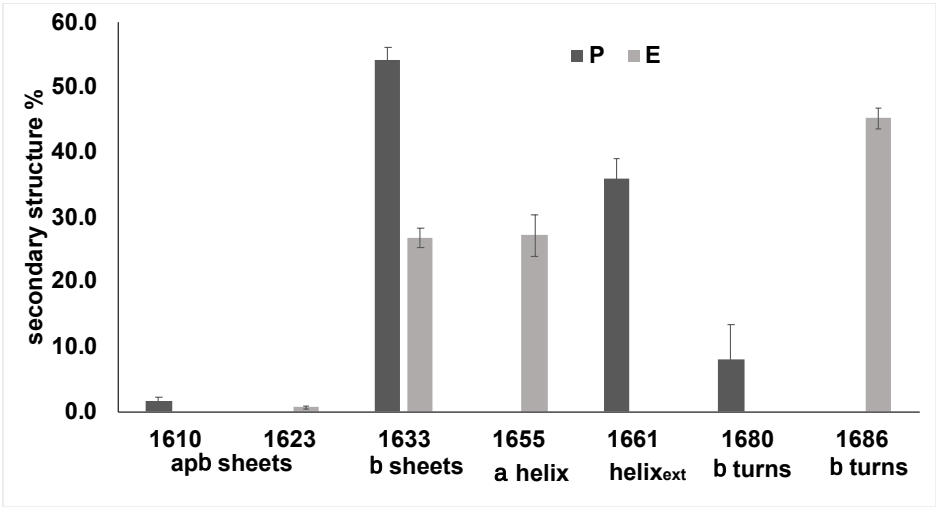

Figure 10. Secondary structure percentages resulting from the deconvolution procedure applied to the amide I region of the FTIR spectra of 4% keratin-filled extruded (E) and printed (P) PLA composites (N=3 replicates).

The comparison with NSK structure clearly evidences a loss of "order" in the structure with the decrease of the antiparallel beta sheets and helix present and a significant increase of beta turns that suggest an organization of the protein filler in the PLA matrix. However, the printing process seems to "recover" a kind of order with the conversion of beta turns into beta sheets and extended helix (component at 1661 cm^{-1}).

3.2.5 Thermic characterization: TG and DSC

The thermal stability of neat PLA and PLA/NSK biocomposites was investigated with TG analysis while the NSK effect on the thermal properties was studied by DSC measurements.
The TG curves obtained and the thermal profiles of printed PLA and PLA/4%NSK are reported in Fig.11 (a) as an example.

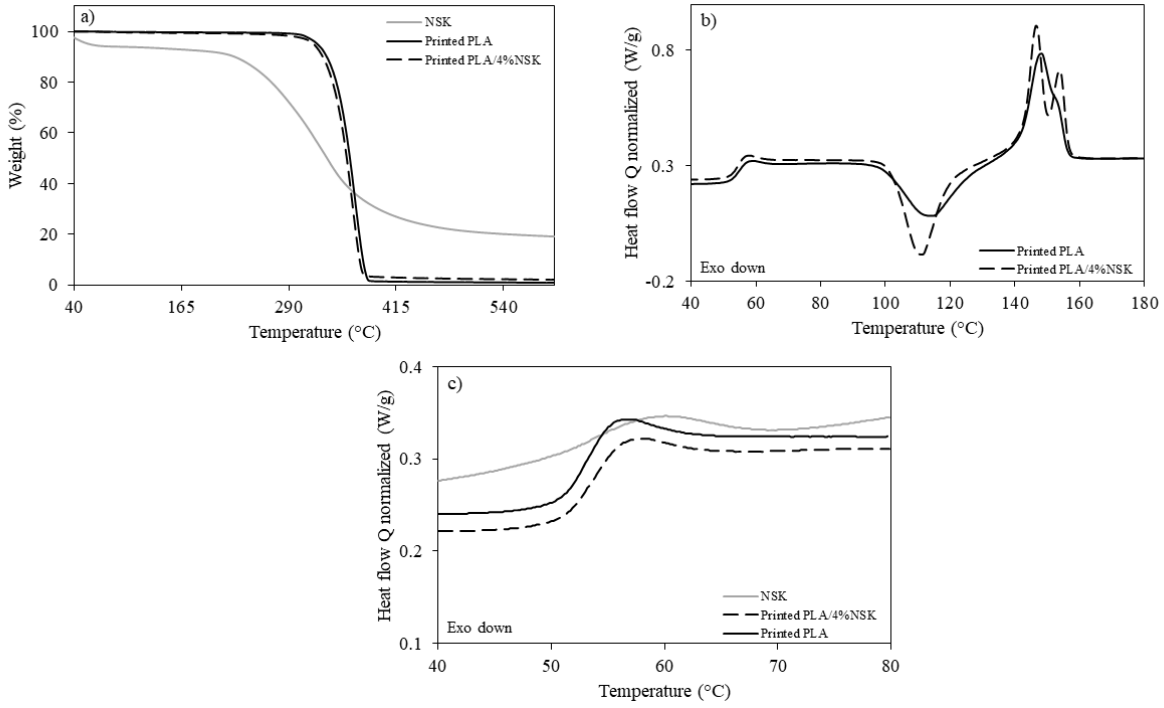

Figure 11. TG (a) and DSC (b-c) curves of printed PLA and PLA/4%KER. The NSK curve is reported as comparison.

The thermal decomposition of PLA occurs mainly in one step, in the temperature range between 290 °C and 400 °C. All biocomposites were found thermally stable until 250 °C and all the polymer matrices were completely decomposed above 400 °C. At 600 °C, for all samples a residue < 2% of both pyrolyzed keratin and PLA was present. Both neat PLA and PLA-filled NSK biocomposites, extruded and printed, did not show any difference, being the curves practically superimposed.

Table 3. Temperatures and mass losses for extruded and printed neat PLA and PLA-filled NSK biocomposites. Replicas have been performed on three representative samples and the results are expressed as mean ± standard deviation.

EXTRUDED	**TEMPERATURE (°C) / (MASS LOSS %W/W)**			
n° step	**PLA**	**PLA/1%NSK**	**PLA/2%NSK**	**PLA/4%NSK**
1	87.9 ± 0.9	86	89	84.06 ± 0.3
	0.22 ± 0.1	0.19	0.3116	0.44 ± 0.02
2	364.8 ± 0.3	366	366	364.0 ± 0.4
	98.6 ± 0.1	98.74	98.14	97.39 ± 0.02
Residue at 600 °C	1.1 ± 0.1	1.1	1.6	2.16 ± 0.03
PRINTED	**PLA**	**PLA/1%NSK**	**PLA/2%NSK**	**PLA/4%NSK**
1	76	68	70	71 ± 3
	0.26	0.29	0.37	0.35 ± 0.03
2	367	369	367	365 ± 3
	98.74	98.22	97.6	98.21 ± 0.07
Residue at 600 °C	0.99	1.49	2.03	1.43 ± 0.07

To verify the homogeneity of the samples, measurements were replicated by sampling in different points of the extruded and printed biocomposites and the results showed good homogeneity (e.g., RSD in extruded PLA/4%NSK is 1%). Moreover, by knowing the composition of the biocomposites and the residues of neat PLA, neat NSK and PLA/NSK materials, it is possible to calculate a theoretical residue. This value compared with the experimental one allows to obtain further information on the homogeneity of the sample and therefore on the compatibility between PLA and keratin. The results reported in Table 4 show that extruded samples are significantly more homogeneous that printed ones (t-test on the residuals, $p = 0.05$). The slightly, but significant, differences that we observe for the printed samples may be due precisely to the printing process, during which the loss of small amount of NSK may occur because of its adhesion to needle's walls.

Table 4. Temperatures corresponding to 5%, 25% and 50% mass-loss, theoretical and experimental residues of extruded and printed PLA and PLA-filled NSK biocomposites.

	Sample	**T (5%) °C**	**T (25%) °C**	**T (50%) °C**	**Theoretical residue**	**Experimental residue**
EXTRUDED	PLA	325	349	360	/	/
	PLA/1%NSK	326	349	361	1.36	1.10
	PLA/2% NSK	325	349	361	1.60	1.56
	PLA/4% NSK	319	345	358	2.10	2.17 ± 0.03
PRINTED	PLA	324	349	361	/	/
	PLA/1%NSK	321	349	362	1.24	1.49
	PLA/2% NSK	319	347	360	1.48	2.04
	PLA/4% NSK	324	349	361	1.98	1.44 ± 0.07

By exploring the temperatures at 5%, 25%, and 50% mass-loss (Table 4), the biocomposites show the same thermal stability of neat PLA. Only the extruded sample with 4% NSK showed a slight decrease in thermal stability, not present in the printed one. These results are in agreement with previous studies of PLA/CF biocomposites containing greater amount of feathers [28,46].

The DSC curve of neat printed PLA showed a glass transition at 53.9 ± 0.1 °C, followed by a cold crystallization at 110.9 ± 0.5 °C and a double peaked melting process (T_{m1} = 147.7 ± 0.7 °C and T_{m2} = 153.3 ± 0.5 °C), (see Figure 4 b and Table 5). The double melting peak was largely reported and discussed in the literature and two models were proposed to explain

this phenomenon [47]. The first is the lamellar thickness model [48,49] and the second one is the melting-recrystallization model [50,51]. The double lamellar thickness model considers the existence of two kinds of crystal lamellae which have different thicknesses and melt at two different temperatures while the melting-recrystallization model proposes that the lower melting temperature is associated with the melting of the lamellae initially present, and the melted material, could recrystallize into a more perfect lamellae which melt at higher temperature.

Table 5. Thermal properties of extruded and printed PLA and PLA-filled NSK biocomposites.

	Sample	T_g (°C)	T_c (°C)	ΔH_c (J/g)	T_{m1} (°C)	T_{m2} (°C)	ΔH_m (J/g)	Xc%
EXTRUDED	PLA	53.6 ± 0.9	108.2 ± 0.5	-21.9 ± 1.0	146.8 ± 0.3	154.7 ± 1.3	22.7 ± 1.1	0.9 ± 0.3
	PLA/1%NSK	55 ± 2	112.0 ± 0.2	-19.6 ± 0.6	147.3 ± 0.2	153.6 ± 0.1	22.8 ± 0.2	3.4 ± 0.5
	PLA/2%NSK	52.8	111.1	-21.5	146.5	153.2	23.8	2.5
	PLA/4%NSK	52.1	108.1	-24.7	145.3	153.4	24.8	0.1
PRINTED	PLA	53.9 ± 0.1	110.9 ± 0.5	-16 ± 3	147.7 ± 0.7	153.3 ± 0.5	20 ± 1	5 ± 2
	PLA/1%NSK	54 ± 1	109.7 ± 0.4	-21.7 ± 0.1	146.6 ± 0.2	153.6 ± 0.1	22 ± 1	0.7 ± 1
	PLA/2%NSK	51.8	109.2	-24.1	145.6	153.1	23.9	-0.2
	PLA/4%NSK	52.4	109.0	-24.4	145.9	153.2	26.1	1.8

Printed PLA showed higher T_c and crystallinity and lower ΔH_c than the extruded one, thus revealing an effect of the printing process on the thermal properties. In fact, the printing process forces semi-molten PLA to flow through a narrow nozzle, and, as shown in a previous study [52], this process induces an orientation of the polymer chains Besides, the printed PLA undergoes a further heat treatment at 205 °C during the printing process and this can cause the increase in crystallinity that is observed respect to extruded PLA. [53]

The effect of NSK on Tg is the same both on extruded and printed samples, i.e., the addition of 1% NSK seems to increase the Tg while the addition of 2% and 4% NSK cause a decrease. Instead, the NSK effect on the crystallinity is opposite. In the extruded samples, NSK up to 2% increases the crystallinity while 4% NSK causes a decrease at 0.1%. Therefore, the NSK effect depends on NSK concentration, particularly we observed a nucleating effect that results in an increased crystallinity when we use up to 2% NSK while with 4% NSK the predominant effect is the hindering of the migration and diffusion of polymer chains to the surface of the growing polymer crystal, lowering crystallinity [54,55].

In the printed sample, the NSK addition always decreased the crystallinity of the material, thus showing only hindering effect. Probably, as a result of the heat treatment at 205 °C, the NSK influences the following PLA crystallization. Actually, Liao et al. [53] observed that after the heat treatment, the PLA crystallinity change is due to transition from the δ form crystallites (imperfect α form) to α form crystallites, therefore, the NSK could hinder this transition not allowing the formation of the more crystalline form (α form).

4. Conclusions

In this study, the production process of completely natural, biodegradable, biocompatible and eco-friendly composite structures was presented. Reusing materials from biowastes which do not decompose freely in nature represents an objective to perform a green and sustainable manufacturing process.
NSK extracted as by product of a microwave assisted acidic extraction from poultry feather was valorized and exploited. The extracted NSK was used as reinforcement filler for the fabrication, by means of HME technology, of NSK-based PLA filaments. As proof of concept these filaments were subsequently 3D printed to highlight applications in the additive manufacturing field. Although in the literature there are many examples of structures fabricated starting from a PLA matrix with keratin fillers, they involve the use of compatibilizers or plasticizers to enhance their physical-chemical properties.
In this study NSK-filled 3D printed PLA structures were produced without the use of any additional compound. Thermal studies highlighted that keratin filled samples maintain the thermal stability as neat PLA samples and found a process type effect (extrusion vs. printing) on thermal properties. Particularly, the 3D printing process leads to an increase of PLA crystallinity, also confirmed by FTIR results. The NSK influence glass transition temperature and PLA crystallinity, showing different effect based on NSK concentration.
From a physico-chemical point of view increased water absorption properties were registered respect to the neat PLA samples. From the mechanical point of view the toughness of NSK-filled PLA samples decreased in line with other literature data. Although a decrease in toughness may appear as a limitation, leading to a more fragile final parts, many researchers on eco-friendly and recycled materials have demonstrated that retaining at least some mechanical properties is sufficient for targeted, many times disposable, applications in packaging, agriculture, medicine, and tissue engineering. Thus, 3D printed PLA/NSK-based biostructuresare in principle suitable for the fabrication of more sophisticated bioproducts at low costs with the aim to drastically short supply chains and biowaste production. In these terms, our one-pot microwave-based keratin extraction process combined with 3D printing can be used in various applications and could potentially serve as alternative for a complete recycle of poultry feathers, as no further byproducts are left, or additional additives are required.

Author contribution statement

Elena Pulidori: Investigation; Data curation; Methodology; Roles/writing – original draft; **Simone Micalizzi:** Investigation; Data curation; Roles/writing – original draft; **Emilia Bramanti**: Investigation; Data curation; Methodology; Writing - review & editing; **Luca Bernazzani:** Data curation, Writing - review & editing; **Carmelo De Maria:** Conceptualization; Data curation; Methodology; Supervision; Writing - review & editing; **Chiara Pelosi:** Conceptualization; Data curation; Methodology; Supervision; Writing - review & editing; **Maria Rosaria Tiné**: Supervision; Writing - review & editing **; Giovanni Vozzi**: Funding acquisition; Supervision; Writing - review & editing; **Celia Duce:** Conceptualization; Data curation; Methodology; Supervision; Writing - review & editing.

Fundings

This work was supported by the European Union's research program MANUNET III under the project KERAPACK MNET17/NMAT-0060.

Ackowledgements

This work was supported by the European Union's research program MANUNET III under the project KERAPACK MNET17/NMAT-0060.

Availability of data and material

Raw data will be made available upon request.

Conflict of interests

The authors declare no conflicts of interests.

Bibliography

1. Sathishkumar TP, Satheeshkumar S, Naveen J. Glass fiber-reinforced polymer composites - A review. J Reinf Plast Compos. 2014;33:1258–75.

2. Patterson BA, Malakooti MH, Lin J, Okorom A, Sodano HA. Aramid nanofibers for multiscale fiber reinforcement of polymer composites. Compos Sci Technol. 2018;161:92–9.

3. Thwe MM, Liao K. Effects of environmental aging on the mechanical properties of bamboo-glass fiber reinforced polymer matrix hybrid composites. Compos - Part A Appl Sci Manuf. 2002;33:43–52.

4. De Luca HG, Anthony DB, Greenhalgh ES, Bismarck A, Shaffer MSP. Piezoresistive structural composites reinforced by carbon nanotube-grafted quartz fibres. Compos Sci Technol [Internet]. Elsevier Ltd; 2020;198:108275. Available from: https://doi.org/10.1016/j.compscitech.2020.108275

5. Ashrafi B, Jakubinek MB, Martinez-Rubi Y, Rahmat M, Djokic D, Laqua K, et al. Multifunctional fiber reinforced polymer composites using carbon and boron nitride nanotubes. Acta Astronaut. 2017;141:57–63.

6. Baldus P, Jansen M, Sporn D. Ceramic fibers for matrix composites in high-temperature engine applications. Science (80-). 1999;285:699–703.

7. Rogovina SZ, Prut E V., Berlin AA. Composite Materials Based on Synthetic Polymers Reinforced with Natural Fibers. Polym Sci - Ser A. 2019;61:417–38.

8. Moslemi AA. Emerging Technologies in Mineral-Bonded Wood and Fiber Composites. Adv Perform Mater. 1999;6:161–79.

9. Mahmud S, Hasan KMF, Jahid MA, Mohiuddin K, Zhang R, Zhu J. Comprehensive review on plant fiber-reinforced polymeric biocomposites [Internet]. J. Mater. Sci. Springer US; 2021. Available from: https://doi.org/10.1007/s10853-021-05774-9

10. Lau K tak, Hoi-yan Cheung K, Hui D. Natural fiber composites. Compos Part B Eng. 2009;40:591–3.

11. Isarankura Na Ayutthaya S, Tanpichai S, Wootthikanokkhan J. Keratin Extracted from Chicken Feather Waste: Extraction, Preparation, and Structural Characterization of the Keratin and Keratin/Biopolymer Films and Electrospuns. J Polym Environ. Springer US; 2015;23:506–16.

12. Sharma, S.; Gupta A. K. Keratin: An Introduction. Springer Ser Polym Compos Mater. Springer, Cham.; 2019. p. 1–18.

13. Donato RK, Mija A. Keratin associations with synthetic, biosynthetic and natural polymers: An extensive review. Polymers (Basel). 2020;12:1–64.

14. Sharma S, Gupta A, Kumar A, Kee CG, Kamyab H, Saufi SM. An efficient conversion of waste feather keratin into ecofriendly bioplastic film. Clean Technol Environ Policy [Internet]. Springer Berlin Heidelberg; 2018;20:2157–67. Available from: https://doi.org/10.1007/s10098-018-1498-2

15. Sinkiewicz I, Śliwińska A, Staroszczyk H, Kołodziejska I. Alternative Methods of Preparation of Soluble Keratin from Chicken Feathers. Waste and Biomass Valorization. 2017;8:1043–8.

16. Esparza Y, Ullah A, Boluk Y, Wu J. Preparation and characterization of thermally crosslinked poly(vinyl alcohol)/feather keratin nanofiber scaffolds. Mater Des [Internet]. Elsevier Ltd; 2017;133:1–9. Available from: http://dx.doi.org/10.1016/j.matdes.2017.07.052

17. Villa ALV, Aragão MRS, dos Santos EP, Mazotto AM, Zingali RB, de Souza EP, et al. Feather keratin hydrolysates obtained from microbial keratinases: Effect on hair fiber. BMC Biotechnol. 2013;13.

18. Pulidori E, Micalizzi S, Bramanti E, Bernazzani L, Duce C, De Maria C, et al. One-pot process:

microwave-assisted keratin extraction and direct electrospinning to obtain keratin-based bioplastic. Macromol Mater engeneering.

19. Chen Y, Geever LM, Killion JA, Lyons JG, Higginbotham CL, Devine DM. Review of Multifarious Applications of Poly (Lactic Acid). Polym - Plast Technol Eng [Internet]. Taylor & Francis; 2016;55:1057–75. Available from: https://doi.org/10.1080/03602559.2015.1132465

20. Arrieta MP, López J, Ferrándiz S, Peltzer MA. Characterization of PLA-limonene blends for food packaging applications. Polym Test [Internet]. Elsevier Ltd; 2013;32:760–8. Available from: http://dx.doi.org/10.1016/j.polymertesting.2013.03.016

21. Vink ETH, Rábago KR, Glassner DA, Gruber PR. Applications of life cycle assessment to NatureWorks™ polylactide (PLA) production. Polym Degrad Stab. 2003;80:403–19.

22. Madhavan Nampoothiri K, Nair NR, John RP. An overview of the recent developments in polylactide (PLA) research. Bioresour Technol [Internet]. Elsevier Ltd; 2010;101:8493–501. Available from: http://dx.doi.org/10.1016/j.biortech.2010.05.092

23. Tyler B, Gullotti D, Mangraviti A, Utsuki T, Brem H. Polylactic acid (PLA) controlled delivery carriers for biomedical applications. Adv Drug Deliv Rev [Internet]. Elsevier B.V.; 2016;107:163–75. Available from: http://dx.doi.org/10.1016/j.addr.2016.06.018

24. Alizadeh-Osgouei M, Li Y, Vahid A, Ataee A, Wen C. High strength porous PLA gyroid scaffolds manufactured via fused deposition modeling for tissue-engineering applications. Smart Mater Med [Internet]. Elsevier Ltd; 2021;2:15–25. Available from: https://doi.org/10.1016/j.smaim.2020.10.003

25. Asim M, Saba N, Jawaid M, Nasir M. Potential of natural fiber/biomass filler-reinforced polymer composites in aerospace applications [Internet]. Sustain. Compos. Aerosp. Appl. Elsevier Ltd; 2018. Available from: http://dx.doi.org/10.1016/B978-0-08-102131-6.00012-8

26. Akampumuza O, Wambua PM, Ahmed A, Li W, Qin XH. Review of the applications of biocomposites in the automotive industry. Polym Compos. 2017;38:2553–69.

27. Fortunati E, Aluigi A, Armentano I, Morena F, Emiliani C, Martino S, et al. Keratins extracted from Merino wool and Brown Alpaca fibres: Thermal, mechanical and biological properties of PLLA based biocomposites. Mater Sci Eng C. Elsevier B.V.; 2015;47:394–406.

28. Huda MS, Schmidt WF, Misra M, Drzal LT. Effect of fiber surface treatment of poultry feather fibers on the properties of their polymer matrix composites. J Appl Polym Sci. 2013;128:1117–24.

29. Tanase CE, Spiridon I. PLA/chitosan/keratin composites for biomedical applications. Mater Sci Eng C [Internet]. Elsevier B.V.; 2014;40:242–7. Available from: http://dx.doi.org/10.1016/j.msec.2014.03.054

30. Cañavate J, Aymerich J, Garrido N, Colom X, Macanás J, Molins G, et al. Properties and optimal manufacturing conditions of chicken feathers/poly(lactic acid) biocomposites. J Compos Mater. 2016;50:1671–83.

31. Aranberri I, Montes S, Azcune I, Rekondo A, Grande HJ. Fully biodegradable biocomposites with high chicken feather content. Polymers (Basel). 2017;9.

32. Mosnáčková K, Šišková AO, Kleinová A, Danko M, Mosnáček J. Properties and degradation of novel fully biodegradable pla/phb blends filled with keratin. Int J Mol Sci. 2020;21:1–15.

33. Flores-Hernandez CG, Velasco-Santos C, Hernandez-Zea AL, Gomez-Guzman O, Yañez-Limon JM, Rivera-Armenta JL, et al. Low Concentrations for Significant Improvements in Thermal and Thermomechanical Properties of Poly(Lactic Acid)–Keratin Biocomposites Obtained by Extrusion and 3D Printing. J Nat Fibers [Internet]. Taylor & Francis; 2020;00:1–14. Available from: https://doi.org/10.1080/15440478.2020.1788483

34. Maniruzzaman M, Boateng JS, Snowden MJ, Douroumis D. A Review of Hot-Melt Extrusion: Process Technology to Pharmaceutical Products. ISRN Pharm. 2012;2012:1–9.

35. Liao R, Yang B, Yu W, Zhou C. Isothermal Cold Crystallization Kinetics of Polylactide/Nucleating Agents. J Appl Polym Sci. 2007;104:310–7.

36. Bramanti E, Bramanti M, Stiavetti P, Benedetti E. A frequency deconvolution procedure using a conjugate gradient minimization method with suitable constraints. J Chemom [Internet]. 1994;8:409–21. Available from: http://doi.wiley.com/10.1002/cem.1180080606

37. Sgarbossa A, Monti S, Lenci F, Bramanti E, Bizzarri R, Barone V. The effects of ferulic acid on β-amyloid fibrillar structures investigated through experimental and computational techniques. Biochim Biophys Acta - Gen Subj [Internet]. Elsevier B.V.; 2013;1830:2924–37. Available from: http://dx.doi.org/10.1016/j.bbagen.2012.12.023

38. Bramanti E, Lenci F, Sgarbossa A. Effects of hypericin on the structure and aggregation properties of β-amyloid peptides. Eur Biophys J. 2010;39:1493–501.

39. Bramanti E, Ferrari C, Angeli V, Onor M, Synovec RE. Characterization of BSA unfolding and aggregation using a single-capillary viscometer and dynamic surface tension detector. Talanta [Internet]. Elsevier B.V.; 2011;85:2553–61. Available from: http://dx.doi.org/10.1016/j.talanta.2011.08.009

40. Senoz E, Wool RP, McChalicher CWJ, Hong CK. Physical and chemical changes in feather keratin during pyrolysis. Polym Degrad Stab [Internet]. Elsevier Ltd; 2012;97:297–307. Available from: http://dx.doi.org/10.1016/j.polymdegradstab.2011.12.018

41. Božič M, Vivod V, Kavčič S, Leitgeb M, Kokol V. New findings about the lipase acetylation of nanofibrillated cellulose using acetic anhydride as acyl donor. Carbohydr Polym. 2015;125:340–51.

42. Barth A. Infrared spectroscopy of proteins. Biochim Biophys Acta - Bioenerg [Internet]. 2007;1767:1073–101. Available from: https://linkinghub.elsevier.com/retrieve/pii/S0005272807001375

43. Kang J, Kim K, Lim YM, Bolander JE. Modeling of fiber-reinforced cement composites: Discrete representation of fiber pullout. Int J Solids Struct [Internet]. Elsevier Ltd; 2014;51:1970–9. Available from: http://dx.doi.org/10.1016/j.ijsolstr.2014.02.006

44. Tissera ND, Wijesena RN, Yasasri H, de Silva KMN, de Silva RM. Fibrous keratin protein bio micro structure for efficient removal of hazardous dye waste from water: Surface charge mediated interfaces for multiple adsorption desorption cycles. Mater Chem Phys [Internet]. Elsevier B.V.; 2020;246:122790. Available from: https://doi.org/10.1016/j.matchemphys.2020.122790

45. Meaurio E, López-Rodríguez N, Sarasua JR. Infrared spectrum of poly(L-lactide): Application to crystallinity studies. Macromolecules. 2006;39:9291–301.

46. Cheng S, Lau K tak, Liu T, Zhao Y, Lam PM, Yin Y. Mechanical and thermal properties of chicken feather fiber/PLA green composites. Compos Part B Eng [Internet]. Elsevier Ltd; 2009;40:650–4. Available from: http://dx.doi.org/10.1016/j.compositesb.2009.04.011

47. Gracia-Fernández CA, Gómez-Barreiro S, López-Beceiro J, Naya S, Artiaga R. New approach to the double melting peak of poly(l-lactic acid) observed by DSC. J Mater Res. 2012;27:1379–82.

48. Cebe P, Su-Don H. Crystallization behavior of poly(ether ether ketone). Polymer (Guildf). 1986;27:1183.

49. Bassett DC, Olley RH, Al Raheil IAM. On crystallization phenomena in PEEK. Polymer (Guildf). 1988;29:1745–54.

50. Jonas AM, Russell TP, Yoon DY. Synchrotron X-ray Scattering Studies of Crystallization of Poly(ether-ether-ketone) from the Glass and Structural Changes during Subsequent Heating-Cooling Processes. Macromolecules. 1995;28:8491–503.

51. Lee Y, Porter R, Lin JS. On the Double-Melting Behavior of Poly (ether ether ketone). Macromolecules. 1989;1760:1756–60.

52. Coppola B, Cappetti N, Maio L Di, Scarfato P, Incarnato L. 3D printing of PLA/clay nanocomposites: Influence of printing temperature on printed samples properties. Materials (Basel). 2018;11:1–17.

53. Liao Y, Liu C, Coppola B, Barra G, Maio L Di, Incarnato L, et al. Effect of Porosity and Crystallinity on 3D Printed PLA Properties. Polymers (Basel). 2019;11:1487.

54. Huda MS, Drzal LT, Mohanty AK, Misra M. Chopped glass and recycled newspaper as reinforcement fibers in injection molded poly(lactic acid) (PLA) composites: A comparative study. Compos Sci Technol. 2006;66:1813–24.

55. Houshyar S, Shanks RA, Hodzic A. The effect of fiber concentration on mechanical and thermal properties of fiber-reinforced polypropylene composites. J Appl Polym Sci. 2005;96:2260–72.